Songklanakarin J. Sci. Technol.
44 (3), 662-667, May - Jun. 2022

http://www.sjst.psu.ac.th

Original Article

Work hardening behavior and model validations for aluminum alloy AA7075

Nakarin Vutipow, Terdsak Arlai, and Patiphan Juijerm*

Department of Materials Engineering, Faculty of Engineering,
Kasetsart University, Chatuchak, Bangkok, 10900 Thailand

Received: 17 May 2021; Revised: 29 November 2021; Accepted: 2 December 2021

Abstract

Work hardening behavior of flow curves of aluminum alloy AA7075 under tensile and compressive loading at room temperature was addressed. The Kocks-Mecking (K-M) and Crussard-Jaoul (C-J) models were applied to analyze the work hardening behavior. Constitutive models, i.e., Hollomon, Ludwigson, Swift, Ludwik, and Voce, were used to predict the flow stresses during tensile/compressive loading. All models were validated, and the empirical parameters were determined by experimental data. The sum of squares of deviations of the prediction (Chi-square, χ^2), coefficient of correlation (R^2) and the mean absolute percentage error (*MAPE*) were calculated to validate simulated flow stresses. It was found that the flow curves exhibited a positive work hardening rate. The K-M plot (work hardening rate versus true stress) showed the work hardening of stage III with a single negative slope value. All models excellently predicted flow stresses with very low *MAPE*. Moreover, a piecewise regression was a meaningful method for accuracy improvement of the models.

Keywords: work hardening, aluminum alloy, flow curve, tension, compression

1. Introduction

Aluminum alloy is a light metal with a one-third density of the ferrous metal. Therefore, it is one of the most important metals, a candidate to replace steels where weight is a concerning issue. Moreover, aluminum alloys possess many attractive properties, i.e., corrosion resistance, formability, high recycling potential. Consequently, aluminum alloys are selected in various industries, i.e., aerospace, automotive, defense, and petrochemical industries. High-strength aluminum alloys in the AA7xxx series were heat-treatable and widely used, especially aluminum alloy AA7075 (Davis, 1993; Lumley, 2011; Polmear, 2005). The principal alloying elements in aluminum alloy AA7075 were zinc (Zn), magnesium (Mg), and copper (Cu). After appropriate precipitation hardening, primary coherent precipitates η' ($MgZn_2$) were distributed and embedded in the aluminium matrix. They obstructed the dislocation movement resulting in strength and hardness enhancement (Davis, 1993; Mason *et al*., 2019; Park & Ardell, 1983; Polmear, 2005). The strength and deformation behavior of aluminum alloys are crucial for manufacturing process, especially for a forming process. However, formability and fracture properties of aluminum alloy AA7075 at room temperature were inferior resulting in part forming limitation in the automotive industry (Lee *et al*., 2020; Palumbo & Tricarico, 2007). Thus, the mechanical properties and work hardening behavior were essential for engineering design and forming process (Embury, Poole, & Lloyd, 2006; Poole, Embury, & Lloyd, 2011). From this point of view, the deformation behavior of the aluminum alloy AA7075 is of particular interest. Understanding the deformation behavior was a path to create a constitutive equation for the flow curve prediction, which is recently much more important in a computer simulation. Currently, many constitutive models were introduced to predict the flow curve. Therefore, in this research, tensile and compression tests were performed on the aluminum alloy AA7075-T651 at room temperature. Flow curves were shown, and work hardening behavior was analyzed using the K-M (Kocks & Mecking, 2003) and C-J models (Crussard & Jaoul, 1950). Flow curves were predicted using constitutive models, i.e., Hollomon, Ludwigson, Swift, Ludwik, and Voce.

*Corresponding author
Email address: fengppj@ku.ac.th

The empirical parameters and equations calculated from experiments were shown. The Chi-square, χ^2, R^2 and the *MAPE* were calculated to validate the constitutive models.

2. Materials and Methods

The aluminum alloy AA7075-T651 was delivered as an aluminum plate with a thickness of 75 mm. The chemical compositions of this alloy are 5.72 Zn, 2.48 Mg, 1.55 Cu, 0.19 Cr, 0.17 Fe, 0.06 Si, 0.02 Mn, 0.02 Ti, and Al balance (all values in wt.%). Specimens with 6×6 mm, and a gauge length of 25 mm were prepared following ASTM E8 for tensile tests. For compressive tests, cylindrical specimens with a diameter of 6 mm, and a height of 13.45 mm were prepared following ASTM E9. The tensile/compressive loading direction corresponds to the rolling direction. Tensile/compressive tests were performed at a constant strain rate of 10^{-3} s^{-1} using a universal testing machine of the Instron, model 5969,

True stress-strain curves of tension and compression were analyzed. The true plastic strain was determined by subtracting the elastic strain from the true total strain. The plastic deformation was analyzed using Hollomon, Ludwigson, Swift, Ludwik, and Voce models. The work hardening behavior was described using K-M and C-J models based on the Ludwik model. All mathematical models and *MAPE* are shown in Equation (1) – (9) as below.

Hollomon (Hollomon, 1945):

$$\sigma = k_H \varepsilon^{n_H} \tag{1}$$

$$\ln \sigma = \ln k_H + n_H \ln \varepsilon \tag{2}$$

Ludwigson (Ludwigson, 1971):

$$\sigma = k_1 \varepsilon^{n_1} + e^{k_2}.e^{n_2 \varepsilon} \tag{3}$$

Ludwik (Ludwik, 1909):

$$\sigma = \sigma_0^L + k_L \varepsilon^{n_L} \tag{4}$$

Crussard–Jaoul (Crussard & Jaoul, 1950):

$$d\sigma/d\varepsilon = d\sigma_0/d\varepsilon + kn\varepsilon^{n-1} \tag{5}$$

$$\ln(d\sigma/d\varepsilon) = \ln\left(kn_{CJ}\right) + \left(n_{CJ} - 1\right)\ln \varepsilon \tag{6}$$

Swift (Swift, 1952):

$$\sigma = k_S(\varepsilon_0 + \varepsilon)^{n_S} \tag{7}$$

Voce (Voce, 1948):

$$\sigma = \sigma_0\left(1 - Ae^{-\beta\varepsilon}\right) \tag{8}$$

where σ is the true stress, ε is the true plastic stress, n is the work hardening exponent, and σ_0, k, A, and β are material constants.

Mean absolute percentage error:

$$MAPE = \frac{1}{n}\sum_{i=1}^{n}\left|\frac{E_i - P_i}{E_i}\right| \times 100 \tag{9}$$

where E is the data from experiments, P is the data from the prediction.

3. Results and Discussion

3.1 Flow curves and work hardening behavior

The true stress-strain curves of the aluminum alloy AA7075-T651 were shown in Figure1. Yield stresses of about 579 and 483 MPa were measured for tension and compression, respectively. The work hardening rate ($d\sigma/d\varepsilon$) were calculated and then plotted versus true stress as K-M plot in Figure 2. After the elasto-plastic transition, the work hardening rate of stage III exhibited a single negative slope value for both tension and compression. It linearly decreased with increasing flow stress until an instability (for tension), where the work hardening rate was equal to the flow stress ($d\sigma/d\varepsilon = \sigma$) (Kang, Kim, Kim, Kwon, & Kim, 2014; Kocks, 1976). It could be mentioned that the plastic deformation was principally associated with the dislocation movement in a single phase because of the single-slope value in the work hardening rate in stage III (Embury *et al*., 2006; Kocks & Mecking, 2003; Mondal, Singh, Mukhopadhyay, & Chattopadhyay, 2013; Poole *et al*., 2011; Sharma, Sree Kumar, Nageswara Rao, & Pathak, 2009). The negative slope in the work hardening rate in stage III indicated that the dynamic recovery occurred concurrently with dislocation generation during the plastic strain even though at room temperature (Embury *et al*., 2006; Poole *et al*., 2011). For multiple phase alloys, i.e., dual-phase steels (ferrite-martensite) or carbon steels (ferrite-pearlite), multiple slope values were observed (Colla *et al*., 2009; Jha, Avtar, Dwivedi, & Ramaswamy, 1987; Mejía, Maldonado, Benito, Jorba, & Roca, 2006). The work hardening behavior could also be described by plotting the work hardening rate versus the true strain or using the C-J model in Equation (6), in which a natural logarithm of the work hardening rate was plotted as a function of a natural logarithm of the true plastic strain, as shown in Figure 3 and Figure 4. The slope of the C-J plot revealed the work hardening exponent, n_{CJ}, in Equation (6). The C-J plot exhibited the single slope value in the work hardening rate in the stage III until reaching the instability as well as necking (for tension). From these results, it could be mentioned that the plastic deformation (dislocation movement) of the aluminum alloy AA7075-T651 occurred in a single phase of aluminum matrix embedded with fine precipitates in a peak-aged condition (Embury *et al*., 2006; Poole *et al*., 2011).

3.2 Flow curve prediction

The flow curves of tension and compression at room temperature were analyzed using various constitutive models. From Equation (2), the n_H of Hollomon model can be determined by the slope of the plot of the natural logarithm of true stress versus the natural logarithm of true plastic. Figure 5(a) illustrated one linear trendline fitting the experimental data from the tensile test. The n_H of about 0.043 was determined with χ^2 of 66.142 and R^2 of 0.922. Flow stresses as a function of plastic strain in Equation (1) were calculated and plotted in Figure 5(b). However, from Figure 5(b), a high deviation of the Hollomon model was observed because of the nonlinear relation in the diagram in Figure 5(a). The nonlinear relation of the natural logarithm of true stress and true plastic strain

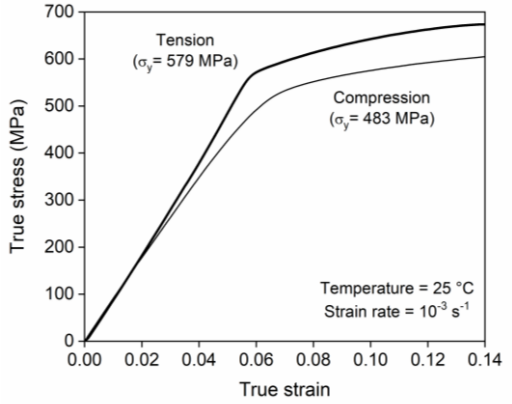

Figure 1. Flow curves of aluminum alloy AA7075 under tensile and compressive loading

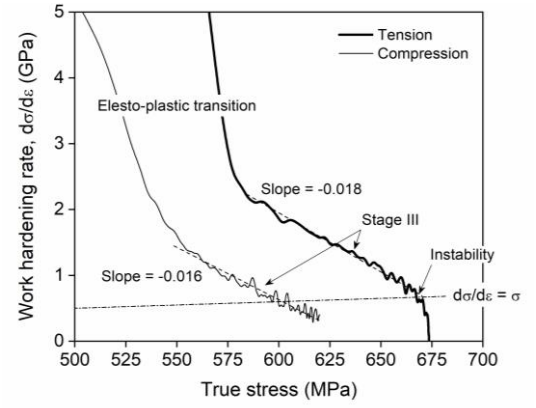

Figure 2. K-M analysis of aluminum alloy AA7075 under tensile and compressive loading

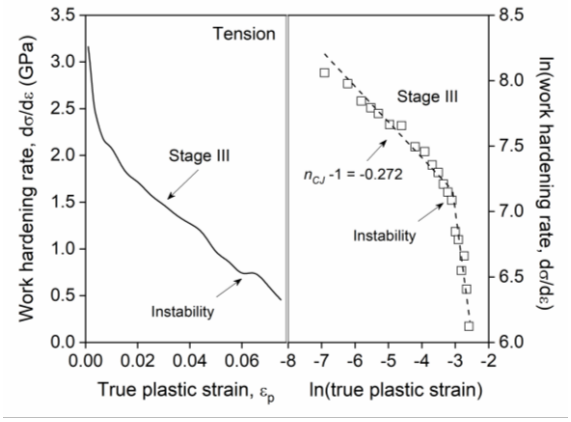

Figure 3. C-J analysis of aluminum alloy AA7075 under tensile loading

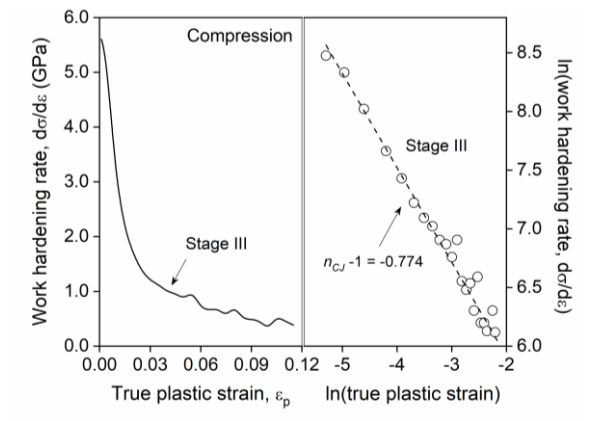

Figure 4. C-J analysis of aluminum alloy AA7075 under compressive loading

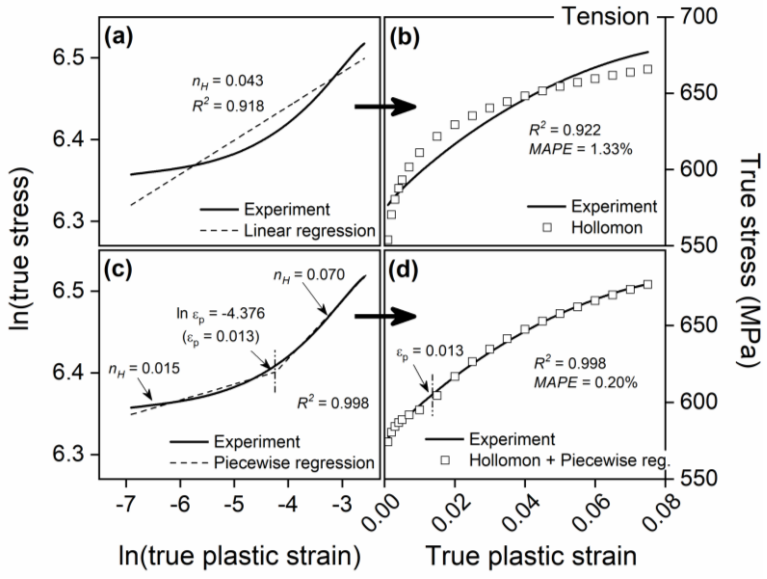

Figure 5. Hollomon analysis and flow curve prediction of aluminum alloy AA7075 under tensile loading: a) determination of *n*-value using linear regression, b) flow curve prediction using *n*-value from linear regression, c) determination of *n*-values using piecewise regression, and d) flow curve prediction using *n*-values from piecewise regression

indicated that the work hardening behavior at slight strain was different. Thus, the piecewise linear function with two segments in Equation (10) and (11) was applied to fit the nonlinear curve of tensile experimental data in Figure 5(a). It was found that the piecewise regression method considerably improved a fitting accuracy, as shown in Figure 5(c) compared with ordinary linear regression in Figure 5(a). Different strength coefficients, k_{H1} and k_{H2} and work hardening exponents, n_{H1} (0.015) and n_{H2} (0.070) were determined using the piecewise regression technique. The lower work hardening exponent, n_{H1} was detected at low plastic strain and corresponded to the planar glide of dislocations. The secondary state with higher work hardening exponent, n_{H2} was corresponded to cross slip of dislocations (Ludwigson, 1971). The transition of the planar glide dislocation to cross slip depending on the dislocation's ability to undergo cross slip (referred to as the stacking fault energy of materials) and temperature. For metallic materials with high stacking fault energy, e.g., aluminum and aluminum alloys, cross slip occurred more easily (Ludwigson, 1971), and the range of the transition should be restricted. For the compression of aluminum alloy AA7075 at room temperature, its plastic deformation behavior was comparable to the tension. Hollomon model for the compression was analyzed and plotted in Figure 6(a)-(d). All strength coefficients and work hardening exponents, χ^2, R^2, and *MAPE* of Hollomon model with and without piecewise regression were summarized in Table 1.

Piecewise linear function with two segments:

$$\ln \sigma = \begin{cases} \ln k_{H1} + n_{H1} \ln \varepsilon\,, & \varepsilon < \varepsilon_i \\ \ln k_{H2} + n_{H2} \ln \varepsilon\,, & \varepsilon \geq \varepsilon_i \end{cases} \tag{10}$$

$$\ln k_{H2} = \ln k_{H1} + (n_{H1} - n_{H2}) \ln \varepsilon_i \tag{11}$$

Table 1. Parameters, empirical constants, χ^2, R^2, and *MAPE* of various models

Model and parameters		Tension	Compression
Hollomon	k_H	743.560	685.594
	n_H	0.043	0.055
	X^2	66.142	32.608
	R^2	0.922	0.980
	MAPE	1.33%	0.68%
Hollomon with piecewise regression	k_{H1}	638.684	596.916
	n_{H1}	0.015	0.031
	ε_i	0.013	0.007
	k_{H2}	810.985	710.899
	n_{H2}	0.070	0.066
	X^2	3.197	3.606
	R^2	0.998	0.998
	MAPE	0.20%	0.22%
Ludwigson	k_1	1016.896	1218.780
	n_1	0.706	0.590
	k_2	6.341	6.142
	n_2	-1.251	-4.327
	X^2	2.106	1.008
	R^2	0.998	0.999
	MAPE	0.19%	0.09%
Ludwik	σ_0^L	565.770	439.740
	k_L	542.899	363.318
	n_L	0.600	0.311
	X^2	2.353	2.540
	R^2	0.998	0.998
	MAPE	0.21%	0.16%
Swift	ε_0	0.022	0.004
	k_s	883.498	728.466
	n_s	0.113	0.076
	X^2	0.776	0.496
	R^2	0.999	0.999
	MAPE	0.10%	0.09%
Voce	σ_0	713.200	604.700
	A	0.194	0.196
	β	18.131	36.040
	X^2	0.119	8.541
	R^2	0.999	0.995
	MAPE	0.05%	0.41%

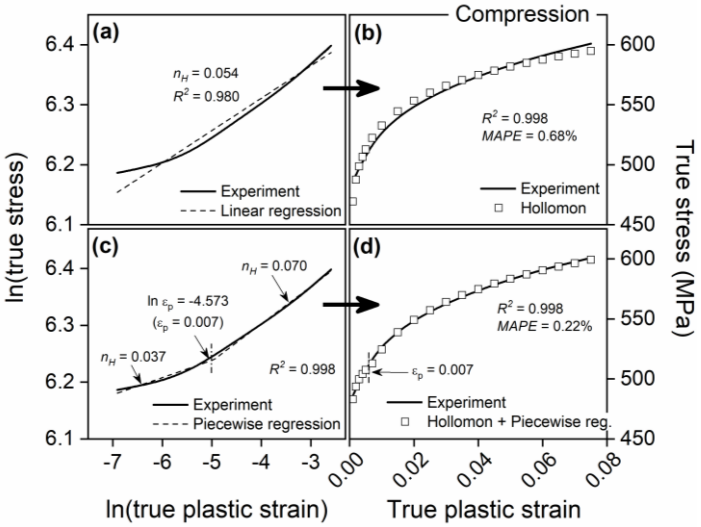

Figure 6. Hollomon analysis and flow curve prediction of aluminum alloy AA7075 under compressive loading: a) determination of *n*-value using linear regression, b) flow curve prediction using *n*-value from linear regression, c) determination of *n*-values using piecewise regression, and d) flow curve prediction using *n*-values from piecewise regression

Ludwigson, Ludwik, Swift, and Voce were excellent constitutive models to fit experimental data of tension and compression of the aluminum alloy AA7075 at room temperature. The model parameters, empirical constants, χ^2, R^2, and *MAPE* of investigated models were determined and summarized in Table 1. Predicted flow curves were plotted and compared with experimental data of the tension and compression of the aluminum alloy AA7075, as shown in Figure 7.

4. Conclusions

In the current investigation, the work hardening behavior of the aluminum alloy AA7075-T651 at room temperature was analyzed. Flow curves were predicted using various constitutive models. Conclusions can be summarized as follows:

1. The aluminum alloy AA7075-T651 exhibited the work hardening rate of stage II and III with a single negative slope value (dynamic recovery) for both tension and compression at room temperature.

2. Hollomon model exhibited high deviation because of the nonlinear relation of the natural logarithm of true stress and true plastic strain of tension and compression of the aluminum alloy AA7075-T651 at room temperature.

3. The piecewise regression was a helpful method to improve the fitting accuracy of the Hollomon model if the natural logarithm of true stress and true plastic strain revealed the nonlinear relation.

4. Constitutive models, Ludwigson, Swift, Ludwik, and Voce excellently predicted the flow curves of tension and compression at room temperature of the aluminum alloy AA7075-T651.

Acknowledgements

Authors would like to gratefully thank the Faculty of Engineering, Kasetsart University, Thailand, for its financial support for N. Vutipow Thanks are also due to U. Rotpai for the support of some investigations.

References

Colla, V., De Sanctis, M., Dimatteo, A., Lovicu, G., Solina, A., & Valentini, R. (2009). Strain hardening behavior of dual-phase steels. *Metallurgical and Materials Transactions A*, *40*(11), 2557. doi:10. 1007/s11661-009-9975-1

Crussard, C., & Jaoul, B. (1950). Contribution à l'étude de la forme des courbes de traction des métaux et à son interprétation physique. *Revue de Métallurgie*, *47*(8), 589–600. doi:10.1051/metal/195047080589

Davis, J. R. (1993). *ASM specialty handbook: Al and Al alloys*. 784.

Embury, J. D., Poole, W. J., & Lloyd, D. J. (2006). The work hardening of single phase and multi-phase aluminium alloys. *Materials Science Forum*, *519*, 71–78.

Hollomon, H. (1945). Tensile deformation. *Aime Trans*, *12*(4), 1–22.

Jha, B. K., Avtar, R., Dwivedi, V. S., & Ramaswamy, V. (1987). Applicability of modified Crussard-Jaoul analysis on the deformation behaviour of dual-phase steels. *Journal of Materials Science Letters*, *6*(8), 891–893. doi:10.1007/BF01729860

Kang, S.-K., Kim, Y.-C., Kim, K.-H., Kwon, D., & Kim, J.-Y. (2014). Constitutive equations optimized for determining strengths of metallic alloys. *Mechanics of Materials*, *73*, 51–57.

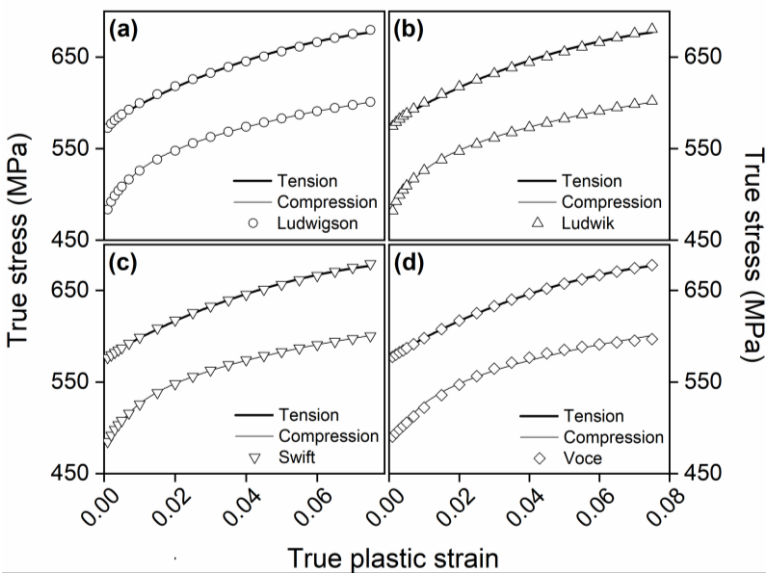

Figure 7. Flow cure predictions of aluminum alloy AA7075 under tensile and compressive loading using (a) Ludwigsion, (b) Ludwik, (c) Swift, and (d) Voce

Kocks, U. F. (1976). Laws for work-hardening and low-temperature creep. *Journal of Engineering Materials and Technology*, *98*(1), 76–85. doi:10.1115/1.3443340

Kocks, U. F., & Mecking, H. (2003). Physics and phenomenology of strain hardening: the FCC case. *Progress in Materials Science*, *48*(3), 171–273.

Lee, J., Bong, H. J., Kim, D., Lee, Y. S., Choi, Y., & Lee, M. G. (2020). Mechanical properties and formability of heat-treated 7000-series high-strength aluminum alloy: Experiments and finite element modeling. *Metals and Materials International*, *26*(5), 682–694. doi:10.1007/S12540-019-00353-9/FIGURES/18

Ludwigson, D. C. (1971). Modified stress-strain relation for FCC metals and alloys. *Metallurgical Transactions*, *2*(10), 2825–2828. doi:10.1007/BF02813258

Ludwik, P. (1909). Elemente der Technologischen Mechanik. *Elemente der Technologischen Mechanik*. doi:10.1007/978-3-662-40293-1

Lumley, R. N. (2011). Introduction to aluminium metallurgy. *Fundamentals of aluminium metallurgy* (pp. 1–19). Amsterdam, The Netherlands: Elsevier.

Mason, C. J. T., Allison, P. G., Rodriguez, O. L., Avery, D. Z., Phillips, B. J., Leah, C., . . . Jordon, J. B. (2019). Plasticity-damage modeling of strain rate and temperature dependence of aluminum alloy 7075-T651. *Journal of Dynamic Behavior of Materials*, *5*(1), 105–114. doi:10.1007/s40870-019-00188-w

Mejía, I., Maldonado, C., Benito, J. A., Jorba, J., & Roca, A. (2006). Determination of the work hardening exponent by the Hollomon and differential Crussard-Jaoul analyses of cold drawn ferrite-pearlite steels. *Materials Science Forum*, *509*, 37–42. doi:10.4028/www.scientific.net/msf.509.37

Mondal, C., Singh, A. K., Mukhopadhyay, A. K., & Chattopadhyay, K. (2013). Tensile flow and work hardening behavior of hot cross-rolled AA7010 aluminum alloy sheets. *Materials Science and Engineering: A*, *577*, 87–100.

Palumbo, G., & Tricarico, L. (2007). Numerical and experimental investigations on the warm deep drawing process of circular aluminum alloy specimens. *Journal of Materials Processing Technology*, *184*(1–3), 115–123.

Park, J. K., & Ardell, A. J. (1983). Microstructures of the commercial 7075 Al alloy in the T651 and T7 tempers. *Metallurgical Transactions A*, *14*(10), 1957–1965. doi:10.1007/BF02662363

Polmear, I. (2005). *Light alloys: from traditional alloys to nanocrystals*. Elsevier.

Poole, W. J., Embury, J. D., & Lloyd, D. J. (2011). Work hardening in aluminium alloys. In *Fundamentals of Aluminium Metallurgy* (pp. 307–344). Amsterdam, The Netherlands: Elsevier.

Sharma, V. M. J., Sree Kumar, K., Nageswara Rao, B., & Pathak, S. D. (2009). Studies on the work-hardening behavior of AA2219 under different aging treatments. *Metallurgical and Materials Tran sactions A: Physical Metallurgy and Materials Science*, *40*(13), 3186–3195. doi:10.1007/s11661-009-0062-4

Swift, H. W. (1952). Plastic instability under plane stress. *Journal of the Mechanics and Physics of Solids*, *1*(1), 1–18. doi:10.1016/0022-5096(52)90002-1

Voce. (1948). The relationship between stress and strain from homogenous deformation. *Journal of the Institute for Metals*, *74*, 537–562.